ELSEVIER

International Journal of Mass Spectrometry 201 (2000) 121–134

International Journal of Mass Spectrometry

Ab initio study of Ar_n–HCO^+ (n = 0–6): insight into size dependent cluster ion properties

K.O. Sullivan[a], Gregory I. Gellene[b,*]

[a]*Department of Chemistry, Creighton University, Omaha, NE 68178, USA*
[b]*Department of Chemistry and Biochemistry, Texas Tech University, Lubbock, TX 79409-1061, USA*

Received 5 October 1999; accepted 19 November 1999

Abstract

Minimum energy structures, dissociation energies, and harmonic vibrational frequencies are determined for Ar_n–HCO^+ (n = 0–6) at the MP2/aug-cc-pVDZ level of theory. In all clusters, one Ar atom occupies an energetically preferred bonding site interacting with the hydrogen of HCO^+ with a linear or near-linear Ar–H–C bond angle. The subsequent Ar atoms add by forming a ring around this Ar–HCO^+ moiety with the detailed geometry determined largely by Ar/Ar interactions. The positions of the first five Ar atoms can be understood in terms of the crystal structure of solid argon whereas the sixth Ar atom produces a five membered Ar ring which has no analog in the solid phase of argon. Nonmonotonic variations in sequential binding energies of the Ar atoms are rationalized in terms of variations in the Ar_n/HCO^+ interaction energy and the differing number of Ar/Ar interactions involved. The HC stretching frequency (ν_1) is found to undergo a large redshift with the first Ar addition and then to slowly blueshift with subsequent Ar additions in agreement with the experimental results. The identities of two previously unassigned combination bands with ν_1 are established and the experimental assignment of a third combination band with ν_1 is confirmed. (Int J Mass Spectrom 201 (2000) 121–134) © 2000 Elsevier Science B.V.

Keywords: Ab initio; Ionic clusters; Ar_n–*HCO^+*; *HCO^+*

1. Introduction

Detailed knowledge of intermolecular interactions is essential for understanding many important physical, chemical, and biological processes [1]. One such interaction, proton bonding [2], has been investigated extensively from a thermodynamic point of view using proton bound dimers, A–H^+–B, as model systems [3–5]. Extending this approach to A–H^+–$B(B)_{n-1}$ species allows more general solvation issues to be addressed. Some obvious questions include whether a special proton bound position will be preserved and if it is, how will the proton bond be modified with an increasing number of B. Two experimental studies which address these questions have focused on Ar_n–HCO^+ [6] and $SiOH^+$–Ar_n [7]. The present work uses ab initio electronic structure techniques to address some of the questions raised in the Ar_n–HCO^+ study.

In the experimental work [6], mass resolved, supersonic jet-cooled Ar_n–HCO^+ (n = 1–13) ions were irradiated with pulsed, tunable infrared radiation in the region of the CH stretch (ν_1) of the HCO^+ chromophore. Optical absorption was detected by monitoring the appearance of fragment ions as a

* Corresponding author.

PII S1387-3806(00)00217-7

function of laser frequency and mass analysis of the daughter ions allowed dissociation pathways to be identified and dissociation energies to be estimated. The molecular origin of the experimentally observed dependence of sequential Ar binding energy, ν_1 vibrational frequency, and three combination bands with ν_1 on cluster size will be addressed by the present work.

The Ar–HCO^+ ion has been addressed by one previous ab initio study [8] using a variety of triple zeta basis sets with electron correlation treated by second and fourth order Møller-Plesset perturbation theory (MP2 and MP4, respectively), and quadratic configuration interaction [QCISD and QCISD(T)] methodologies. However, because binding of only a single Ar was considered, the various cluster size dependent properties could not be addressed.

2. Computation methods

In choosing a computational model to study the Ar_n–HCO^+ series, the accuracy benefits provided by large basis sets and high levels of electron correlation were weighed against the computational resource and time costs. In the previous ab initio study, Nowek and Leszczyński [8] established that MP2 harmonic frequencies for Ar–HCO^+ agreed with the QCISD values to within about 1% for bending modes and the C–H stretching mode (ν_1) and to within about 3%–4% for the Ar–HCO^+ and the C≡O stretching modes. Furthermore, that work also showed that the MP2 D_0 for Ar–HCO^+ differed from the QCISD(T) value by only 2.9%. This level of agreement was judged sufficient to study the cluster dependent trends in vibrational frequencies and binding energies, and an MP2 methodology was adopted. However, Nowek and Leszczyński employed triple zeta basis sets which are prohibitively large for use with multiple Ar containing cluster ions. Instead, Dunning's correlation consistent polarized valence double zeta basis set augmented with diffuse functions (aug-cc-pVDZ) was used. The diffuse function augmentation is particularly important for describing the polarization of Ar which is primarily responsible for the attractive interaction with HCO^+ and other Ar atoms. Even with the use of a double zeta basis set, practical considerations limited the present study to 0–6 Ar atoms; a smaller range than the 0–13 Ar atoms studied experimentally [6]. In addition, only relatively high symmetry geometric structures for Ar_6–HCO^+ could be studied. Possible errors caused by using a double zeta basis set will be assessed by comparing MP2/aug-cc-pVDZ and MP2/aug-cc-pVTZ (an augmented triple zeta basis set) results for HCO^+, Ar–HCO^+, and Ar_2–HCO^+.

Basis set superposition error (BSSE) is a concern for computational estimates of interaction energies in general, and dissociation energies in particular, for weakly bound complexes especially when using a double zeta basis set. This problem is often addressed by the functional counterpoise correction (ΔE_{CP}) of Boys and Bernardi [9] which for an atomic dimer (AB) is given by

$$\Delta E_{CP} = E_A(\chi_A) + E_B(\chi_B) - E_A(\chi_A\chi_B) - E_B(\chi_A\chi_B) \quad (1)$$

where $E_A(\chi_A)$ is the energy of A calculated only with the basis functions centered on A, $E_A(\chi_A\chi_B)$ is the energy of A calculated with the basis functions centered on A and B but without the electrons or nuclear charge associated with B, and analogous definitions for $E_B(\chi_B)$ and $E_B(\chi_A\chi_B)$. In this approach, a BSSE corrected dissociation energy is given by

$$D_e(\mathrm{CP}) = D_e - \Delta E_{CP} \quad (2)$$

ΔE_{CP} is dependent on the internuclear separation (or geometry in general) because this distance specifies the relative location of the basis functions centered on A and B. If one of the subunits is molecular (as it is in the present study), an additional geometry dependence to ΔE_{CP} is introduced because the geometry of the molecular subunit in the cluster environment is generally different than its isolated geometry. This geometry effect can be accounted for by calculating the energy terms in Eq. (1) with the appropriate distortion of the molecular subunit. This approach is

Table 1
Properties of Ar, Ar_2, and Ar_3 calculated with MP2 theory and experimental comparisons

Property	Basis set			Expt.
	aug-cc-pVDZ	aug-cc-pVTZ	aug-cc-pVQZ	
Ar				
Polarizibility (a_0^3)	9.76	10.81	11.10	11.08[a]
Ar_2				
r_e (Å)	3.9038	3.7657	3.7529	3.761[b]
$\omega_e(\sigma_g)$ (cm^{-1})	24.96	32.04	31.73	30.68[b]
D_e (cm^{-1})	88.76	111.01	112.83	99.2[b]
D_e(CP) (cm^{-1})	55.04	83.23	97.51	
Ar_3				
r_e (Å)	3.9191	3.7615	3.7497	~3.761[c]
$\omega_e(a_1')$ (cm^{-1})	31.07	39.96	38.99	
$\omega_e(e')$ (cm^{-1})	22.42	28.13	28.40	
D_e (cm^{-1})[d]	267.28	333.80	339.90	~297[c]
D_e(CP) (cm^{-1})[d]	167.99	252.15	295.00	

[a] See [10].
[b] See [11].
[c] See [15] and [16].
[d] D_e is measured with respect to 3Ar.

readily generalized to a complex containing n subunits with the result

$$\Delta E_{CP} = \sum_{i}^{n} [E_{A_i}(\chi_{A_i}) - E_{A_i}(\chi_{A_1}\chi_{A_2} \cdots \chi_{A_n})] \quad (3)$$

In addition, the consequences of using a finite basis set were explored by comparing polarizability, equilibrium geometries, and harmonic frequencies for Ar, Ar_2, and Ar_3 calculated at the MP2 level using Dunning's series of augmented double, triple, and quadruple (aug-cc-pVQZ) zeta basis. For brevity, these basis sets will be denoted as pVDZ+, pVTZ+, and pVQZ+, respectively. These calculations will also help calibrate the Ar_n contribution to the total interaction energy of Ar_n–HCO^+ complexes calculated at the MP2/pVDZ+ level.

In general, stationary points on the Ar_n–HCO^+ hypersurfaces were located and characterized with MP2/pVDZ+ calculations with frozen core electrons. Analytical first derivatives were used to optimize structures to a residual root-mean-square force of less than 10^{-6} Hartree/bohr and analytical second derivatives were used to characterize a stationary point as a local minimum (all real harmonic frequencies) or a transition state (one imaginary harmonic frequency). All calculations were performed using the GAUSSIAN 94 suite of codes running on a DEC alpha 3000/700 workstation. In all calculations, pure spherical harmonic basis functions were used.

3. Results

3.1. Ar

Properties for Ar, Ar_2, and Ar_3 calculated using MP2 theory with the pVDZ+, pVTZ+, and pVQZ+ basis sets are summarized and compared to available experimental information in Table 1. For Ar, the calculated polarizability smoothly approaches the experimental value as the basis set size increases with the MP2/pVQZ+ result agreeing extremely well with the experimental value [10]. However, the calculated polarizability at the level where most of the current work is done (MP2/pVDZ+) is about 12% low.

3.2. Ar_2

For Ar_2, the calculated equilibrium bond length (r_e) decreases with increasing basis set size with the largest change occurring between the pVDZ+ and pVTZ+ values. Again, the pVQZ+ value agrees very well with the experimental values [11] differing by less and 0.005 Å. The calculated dissociation energy measured from the minimum of the electronic potential curve (D_e) increases with increasing basis set size with the largest change again occurring between the pVDZ+ and pVTZ+ values. As anticipated, BSSE is an important consideration. When BSSE is accounted for by Eq. (1), D_e(CP) is decreased from the D_e value by 33.72 cm^{-1} (38%), 27.89 cm^{-1} (25%), and 15.32 cm^{-1} (14%) for calculations performed with the pVDZ+, pVTZ+, pVQZ+ basis sets, respectively. As expected, the absolute and relative magnitude of this correction decreases with increasing basis set size. The harmonic frequencies calculated with the pVTZ+ and pVQZ+ basis sets are very similar, agree well with the experimental value [11], and are about 7 cm^{-1} greater than the pVDZ+ value.

3.3. Ar_3

The equilibrium geometry of Ar_3 is an equilateral triangle (D_{3h} point group). With each basis set investigated, the Ar–Ar separation was very nearly the same as the respective r_e calculated for Ar_2. Similarly, for the three basis sets, the calculated D_e and D_e(CP) calculated using Eq. (3) were found to be within 3 cm^{-1} of three times the corresponding value calculated for the Ar_2. As was the case with Ar_2, the pVTZ+ and pVQZ+ harmonic vibrational energies are very similar and about 6–9 cm^{-1} greater than those calculated with the pVDZ+ basis set.

3.4. HCO^+

Properties for HCO^+ and Ar–HCO^+ calculated at the MP2 level with pVDZ+ and pVTZ+ basis sets are summarized and compared to the available experimental information in Table 2. The HCO^+ ion is found to be linear with both basis sets with the HC and CO bond lengths decreasing by about 0.01 Å as the basis set is increased from pVDZ+ to pVTZ+. The pVTZ+ values are slightly larger than the experimental results [12]. Harmonic frequencies for the HC stretching (ω_1), HCO bending (ω_2), and CO stretching (ω_3) modes are changed slightly by increasing the basis set size (−7.7, +12.0, and +30.4 cm^{-1}, respectively).

3.5. $Ar–HCO^+$

Calculated minimum energy structures for Ar_n–HCO^+ ions, n = 1–6, are shown in Fig. 1. The Ar–HCO^+ ion is found to be linear with Ar binding on the hydrogen end of the HCO^+ ion in agreement with previous experimental [6,13] and theoretical [8] results. The r_e values again decrease with increasing basis set size with the largest effect observed for r_e(HAr) which decreases by about 0.065 Å. The CH stretch (ω_1) decreased by about 54 cm^{-1} with increasing basis set size which is a considerably larger effect than that observed for HCO^+. Also, ω_4, the Ar–HCO^+ stretch, shows a significant basis set dependence increasing by 18 cm^{-1} (15%) when the basis set is changed from pVDZ+ to pVTZ+. As was the case for HCO^+, the bending modes (ω_2 and ω_5) are fairly insensitive to basis set size. Increasing basis set size from pVDZ+ to pVTZ+ increases D_e by about 170 cm^{-1} and, with the expected decrease in ΔE_{CP}, D_e(CP) increases by about 300 cm^{-1}.

3.6. $Ar_2–HCO^+$

Two geometric structures for Ar_2–HCO^+ were investigated. The first was a symmetric C_{2v} structure where each of the Ar atoms interacted equivalently with the hydrogen of a linear HCO^+. This structure proved to be a first order transition state and motion initiated along the normal mode associated with the imaginary frequency led to the global minimum: a C_s structure which can be described as a near linear Ar–HCO^+ (θ_{ArHC} = 177.6°, θ_{HCO} = 178.6°) interacting with the second Ar atom. The second Ar atom is located about equidistance from the H and C atoms with an Ar–Ar distance very close to the r_e of Ar_2.

Table 2
Properties of HCO^+ and Ar–HCO^+ calculated with MP2 theory and experimental comparisons

Property	Basis set		Expt.
	aug-cc-pVDZ	aug-cc-pVTZ	
HCO^+			
r_e(HC) (Å)	1.1020	1.0911	1.0929[a]
r_e(CO) (Å)	1.1295	1.1192	1.1072[a]
$\omega_1(\sigma)$ (cm^{-1})	3244.2	3236.5	3088.7[b]
$\omega_2(\pi)$ (cm^{-1})	835.0	842.0	828[c]
$\omega_3(\sigma)$ (cm^{-1})	2098.3	2128.7	2183.9[d]
Ar–HCO^+			
r_e(HC) (Å)	1.1158	1.1082	
r_e(CO) (Å)	1.1299	1.1199	1.092[e]
r_e(HAr) (Å)	2.1871	2.1222	2.157[e]
$\omega_1(\sigma)$ (cm^{-1})	3035.4	2981.7	2815.1[f]
$\omega_2(\pi)$ (cm^{-1})	920.4	925.3	
$\omega_3(\sigma)$ (cm^{-1})	2075.2	2098.0	2135.7[g]
$\omega_4(\sigma)$ (cm^{-1})	120.1	138.1	131[h]
$\omega_5(\pi)$ (cm^{-1})	131.0	132.1	109[h]
D_e (cm^{-1})[i]	1611.5	1781.3	
D_e(CP) (cm^{-1})[i]	1227.6	1528.7	
ΔZPE (cm^{-1})[j]	−160.7	−142.0	

[a] See [12].
[b] ν_1 value [19].
[c] ν_2 value [24].
[d] ν_3 value [20].
[e] r_s value [12].
[f] ν_1 value [6].
[g] ν_3 value [23].
[h] See [13].
[i] With respect to Ar + HCO^+.
[j] ZPE(HCO^+) − ZPE(Ar–HCO^+).

This pattern of one Ar occupying a preferred near linear Ar–H–C position will be a common theme for all the Ar_n–HCO^+ ions investigated and this Ar atom will be denoted Ar*. The additional Ar atoms which are positioned nearly equidistant from the C and H atoms with be denoted as "ring" Ar. The rationale for this label will become clear as the larger Ar cluster ions are discussed. Variations of the geometric properties with basis set size are similar to what has been observed previously and are summarized in Table 3. In contrast to Ar–HCO^+, increasing basis set size causes the HC stretch (ω_1, Table 3) to increase slightly. Similar to Ar–HCO^+, the bending modes of HCO (ω_2 and ω_3, Table 3) and the CO stretch (ω_4, Table 3) are slightly changed by the basis set size increase. Also similar is the approximate 15% increase in the Ar–HCO stretching (ω_5, Table 3) vibrational energy when the basis set increases from pVDZ+ to pVTZ+.

3.7. Ar_3–HCO^+

Two geometric structures were also investigated for Ar_3–HCO^+. The first was a symmetric C_{2v} structure where two ring Ar atoms interacted equivalently with a linear Ar–HCO^+ moiety. This structure very much resembled the minimum energy Ar_2–HCO^+ structure with the third Ar located opposite the ring Ar. Although the MP2/pVDZ+ calculations predicted that this structure was a local minimum, the bending mode bringing the two ring Ar atoms closer together was associated with only a 5.4 cm^{-1} vibrational energy. Continued motion along this coordinate ultimately led to a structure which was more stable by

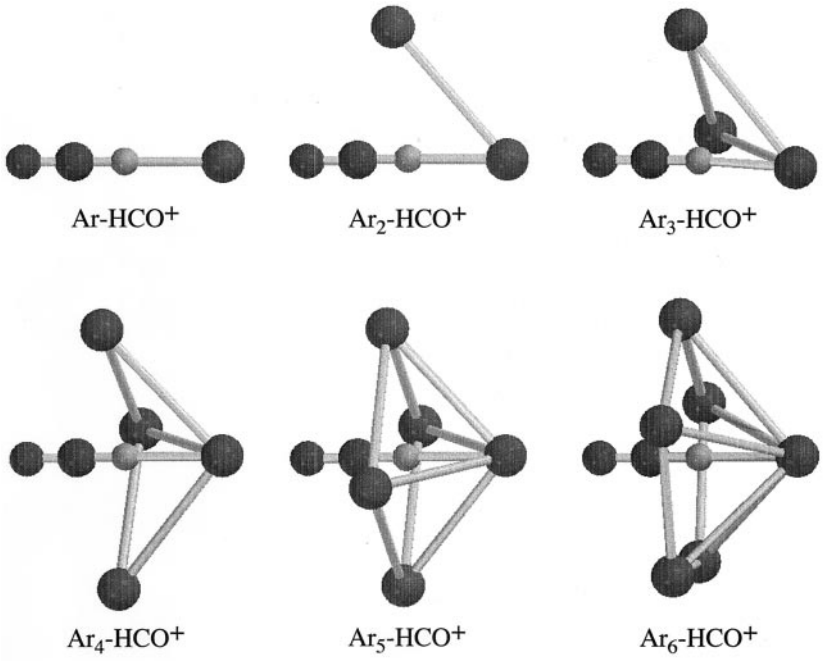

Fig. 1. Minimum energy structures for Ar_n–HCO^+, $n = 1$–6, cluster ions calculated at the MP2/aug-cc-pVDZ level of theory.

about 100 cm^{-1}. This global minimum energy structure has a C_s geometry where the two ring Ar atoms interact equivalently with a near linear Ar–HCO^+ and are separated by about 3.975 Å. Selected geometric parameters calculated for the C_s global minimum at the MP2/pVDZ+ level are summarized in Table 4.

3.8. Ar_4–HCO^+

Two geometric structures were also investigated for Ar_4–HCO^+. The first was a symmetric C_{3v} structure where three ring Ar atoms interacted equivalently with a linear Ar–HCO^+ moiety. This structure was found to be a second order transition state with a twofold degenerate imaginary frequency associated with motion of the ring Ar atoms. Motion along the normal coordinates associated with these frequencies leads to a C_s global minimum energy structure where two of the previously equivalent ring Ar distances decreased form 5.126 to 3.969 Å while the third increased to 5.904 Å. The energy of this global minimum is about 132 cm^{-1} lower than the C_{3v} transition state. Selected geometric parameters calculated for the C_s global minimum at the MP2/pVDZ+ level are summarized in Table 4.

3.9. Ar_5–HCO^+

Only a single geometric structure was investigated for Ar_5–HCO^+. This structure had a symmetric C_{4v} geometry with four ring Ar atoms interacting equivalently with a linear Ar–HCO^+ moiety. The ring Ar separations in this minimum energy structure are about 0.25 Å larger than the r_e for Ar_2. Selected geometric parameters calculated for the C_{4v} global minimum at the MP2/pVDZ+ level are summarized in Table 4.

3.10. Ar_6–HCO^+

Two geometric structures were investigated for Ar_6–HCO^+. The first was a symmetric C_{4v} structure consisting of the minimum energy-like structure for Ar_5–HCO^+ with the additional Ar atom interacting with the O atom forming a linear Ar–HCO^+ moiety. However, this structure was found to have about 1700

Table 3
Properties of Ar_2–HCO^+ calculated with the MP2 theory

Property	Basis set	
	aug-cc-pVDZ	aug-cc-pVTZ
r_e(HC) (Å)	1.1130	1.1049
r_e(CO) (Å)	1.1301	1.1202
r_e(HAr*) (Å)	2.2029	2.1378
r_e(Ar*Ar) (Å)	3.9214	3.8051
$\omega_1(a')$ (cm^{-1})	3005.0	3016.5
$\omega_2(a')$ (cm^{-1})	887.2	895.7
$\omega_3(a'')$ (cm^{-1})	915.6	920.9
$\omega_4(a')$ (cm^{-1})	2078.7	2102.3
$\omega_5(a')$ (cm^{-1})	119.8	137.0
$\omega_6(a')$ (cm^{-1})	130.2	130.4
$\omega_7(a')$ (cm^{-1})	174.7	183.1
$\omega_8(a')$ (cm^{-1})	69.8	72.9
$\omega_9(a')$ (cm^{-1})	31.9	35.3
D_e (cm^{-1})[a]	2633.8	2910.4
D_e(CP) (cm^{-1})[a]	2068.2	2549.3
D_e(CP′) (cm^{-1})[a]	2094.8	2567.3
ΔZPE (cm^{-1})[b]	−230.4	−222.5

[a] With respect to 2Ar + HCO^+.
[b] ZPE(HCO^+) − ZPE(Ar_2–HCO^+).

cm^{-1} higher energy than a C_{5v} structure which has five equivalent ring Ar atoms interacting with a linear Ar–HCO^+.

4. Discussion

4.1. Ar clusters

As stated previously, the Ar cluster calculations were performed to help calibrate the reliability of the MP2/pVDZ+ results for Ar_n–HCO^+ clusters. In particular, the results in Table 1 allow questions about the dependence of dissociation energies and harmonic frequencies on basis set size to be addressed quantitatively. The MP2/pVDZ+ polarizability for Ar is about 12% low [10] suggesting that the Ar_2 interaction energy calculated at this level may be more than 20% low [1]. Nevertheless, this D_e for Ar_2 is surprisingly good, being only about 11% low. However, the quality of this result seems to arise from a fortuitous cancellation of errors. The value of D_e(CP) suggests that as much as 38% of the MP2/pVDZ+ binding energy for Ar_2 may be due to BSSE. Furthermore, the value of D_e for Ar_2 calculated at the MP2/pVTZ+ and MP2/pVQZ+ levels suggests that MP2 theory may overestimate the Ar_2 binding energy. This conclusion is supported by selected calculations of Ar and Ar_2 at the MP4(SDTQ)/pVTZ+ level which indicated

Table 4
Properties of Ar_{3-6}–HCO^+ calculated at the MP2/aug-cc-pVDZ level

Property	Ar_3–HCO^+	Ar_4–HCO^+	Ar_5–HCO^+	Ar_6–HCO^+
Point group	C_s	C_s	C_{4v}	C_{5v}
r_e(HC) (Å)	1.1105	1.1083	1.1058	1.1069
r_e(CO) (Å)	1.1303	1.1304	1.1306	1.1303
r_e(HAr*) (Å)	2.2148	2.2258	2.2444	2.2115
r_e(HAr) (Å)	2.9571	2.9527	2.9529	3.1008
r_e(HAr′)[a] (Å)		2.9791		
r_e(Ar*Ar) (Å)	3.9224	3.8904	3.8582	4.0066
r_e(Ar*Ar′)[a] (Å)		3.9262		
r_e(ArAr) (Å)	3.9749	5.9037	4.1608	3.6219
r_e(ArAr′)[a] (Å)		3.9695		
θ(Ar*HC)	178.0°	178.4°	180.0°	180.0°
θ(HCO)	176.5°	177.3°	180.0°	180.0°
D_e (cm^{-1})[b]	3738.9	4827.2	5985.6	6794.2
D_e(CP) (cm^{-1})[b]	2800.8	3760.3	4603.0	5185.6
D_e(CP′) (cm^{-1})[b]	3007.1	3953.5	4807.1	5495.2
ΔZPE (cm^{-1})[c]	−316.0	−395.1	−482.8	−531.1

[a] Prime denotes the symmetry distinct ring Ar atom.
[b] With respect to nAr + HCO^+.
[c] ZPE(HCO^+) − ZPE(Ar_n–HCO^+).

that the MP2 calculations may overestimate the binding energy by about 13%. This accidental ability of MP2/pVDZ+ calculations to provide a good description Ar–Ar interaction energy in Ar_2 is seen in Table 1 to apply also to Ar_3. This result is again fortuitous because the MP2 theory is not capable of describing the three body interaction terms [14] which would normally be important. However, the Ar_3 potential near the equilibrium geometry is dominated by two body interactions [15] (which are accidentally described well) with the three body terms accounting for only about 2 cm^{-1} of repulsion [16]. Although MP2/pVDZ+ calculations is getting the "right" Ar cluster interaction energy for the "wrong" reasons, the situation can be exploited in the present study. Thus, the first lesson to be learned from Table 1 is that dissociation energies calculated at the MP2/pVDZ+ level should be compared to experimental values without the counterpoise correction to Ar–Ar interactions. From this point of view, a modified functional counterpoise correction ($\Delta E_{CP'}$) for the Ar_n–HCO^+ cluster ions, valid for MP2/pVDZ+ calculations, is given by

$$\Delta E_{CP'} = E_{HCO^+}(\chi_{HCO^+}) + E_{(Ar)_n}(\chi_{Ar_1}\chi_{Ar_2}\cdots\chi_{Ar_n}) - E_{HCO^+}(\chi_{HCO^+}\chi_{Ar_1}\chi_{Ar_2}\cdots\chi_{Ar_n}) - E_{(Ar)_n}(\chi_{HCO^+}\chi_{Ar_1}\chi_{Ar_2}\cdots\chi_{Ar_n}) \quad (4)$$

where $(Ar)_n$ denotes the n Ar atoms in the geometrical arrangement they adopt in the Ar_n–HCO^+ cluster ion.

The MP2/pVTZ+ and MP2/pVQZ+ calculations for the harmonic vibrational energy of Ar_2 agree very well with the experimental value [11]. However, the importance of anharmonicity in this molecule decreases the value of harmonic vibrational energies for predicting excitation energies. For example, the experimental $\Delta G_{v+1/2}$ values are 25.69, 20.58, 15.58, 10.91, and 6.84 cm^{-1} for $v = 0$–4, respectively [11]. Interestingly, the MP2/pVDZ+ harmonic vibrational energy (24.96 cm^{-1}) is very close to the experimental $v = 1 \leftarrow v = 0$ transition energy (25.69 cm^{-1}). For Ar_3, neither experimental harmonic nor actual transition energies are available. However, considering that the interaction potential is overwhelming dominated by two-body forces [15,16], it seems likely that the MP2/pVQZ+ calculations will provide a good estimate of the harmonic frequencies. But again, the importance of anharmonicity diminishes the relevance of harmonic transition energies in making experimental comparisons. Wright and Hutson [17] have recently calculated nearly all of the bound vibrational levels for Ar_3 with $J = 0$ using an accurate potential energy surface. They find "$v = 1$" ← "$v = 0$" transition energies of 30.6 and 22.5 cm^{-1} for the a_1' and e' modes, respectively. These values are extremely close to the MP2/pVDZ+ harmonic vibrational energies of 31.07 and 22.42 cm^{-1}, respectively. It would appear that for Ar_2 and Ar_3 the deficiencies in MP2/pVDZ+ calculations of harmonic vibrational energies is accidently nearly equal to the anharmonic effects operating on the fundamental transition energy so that the MP2/pVDZ+ calculations provide a high quality estimate of the actual fundamental transition energy. Thus, the second lesson to be learned from Table 1 is that $v = 1 \leftarrow v = 0$ vibrational transition energies for modes of Ar_n–HCO^+ clusters which are dominated by motion of the Ar atoms, may be reliably predicted by MP2/pVDZ+ calculations.

4.2. Ar_n–HCO^+ clusters

Although the results were presented with each system distinguished by the number of Ar atoms present, instructive trends in the results can be identified by regrouping systems under the headings of geometric configuration, dissociation energy, fundamental band energies, and combination band energies. It is also instructive to consider the relative energetics for stepwise addition of each Ar atom which can be determined from the information in Tables 2–4. Insights gained from the MP2/pVTZ+ calculations for HCO^+, Ar–HCO^+, and Ar_2–HCO^+ will be discussed as appropriate.

4.2.1. Geometric configurations

The first Ar atom interacts with the hydrogen atom of HCO^+ forming a linear Ar–HCO^+. The experimental results [6] were interpreted in terms of a special stability for this first bonding position which was essentially preserved as additional Ar atoms

bonded to the cluster. This conclusion is completely supported by the present computations which find that the Ar*–H–C angle is never less than 178° for any of the minimum energy structures of the Ar_n–HCO^+ cluster ions investigated. The uniqueness of this bonding position is emphasized by the Ar*–H distance being approximately 0.7 Å shorter than the other Ar–H distances in the $n = 2$–6 cluster ions. As the cluster grows from $n = 1$ to $n = 4$, all the nearest neighbor Ar–Ar distances are remarkably similar being only slightly larger (0.02–0.07 Å) than the r_e of Ar_2 calculated at the same level of theory. The association of these Ar–Ar distances with the r_e of Ar_2 is supported by the the MP2/pVTZ+ calculations where the Ar–Ar distances contract by nearly equal amounts (0.14 Å for Ar_2; 0.12 Å for Ar_2–HCO^+) relative to the MP2/pVDZ+ values. These results suggest that following the bonding of the first Ar to the special linear Ar–H–C site, the position of the subsequent Ar atoms is significantly influenced by Ar–Ar interactions. Indeed, the addition of each Ar atom up to $n = 5$ occupy "face-centered" positions of the face centered cubic crystal structure of solid argon [18]. Support for interpreting these structures in terms of the argon crystal lattice structure is provided by the 96.1° bond angle of the three ring Ar atoms in Ar_4–HCO^+. This bond angle is not constrained by the geometric symmetry of Ar_4–HCO^+ and is nevertheless close to the 90° angle found in the crystal. However, this structure pattern is abandoned in the Ar_6–HCO^+ cluster ion because it is not possible to interpret a five membered Ar ring as a component of the argon crystal [18]. Thus, the C_{5v} structure for the Ar_6–HCO^+ ion is uniquely a small cluster, gas phase result. It would be interesting to have argon matrix isolated HCO^+ infrared spectra to compared to the gas phase cluster results because it would seem likely that the crystal forces in the argon solid matrix would prevent a five member Ar ring from forming around the HCO^+ ion.

4.2.2. Dissociation energies

Experimental sequential dissociation energies were determined form the observed fragment ion intensity distributions by two different modeling procedures [6]. The first procedure assumed that the available energy was statistically distributed among the dissociation coordinate and the other internal degrees of freedom. The second procedure assumed that the first Ar atom ejected from the cluster left with near zero kinetic energy. This model was motivated by noting that the ν_1 (3088.7 cm^{-1} [19]) and ν_3 (2183.9 cm^{-1} [20]) vibrational energy difference for HCO^+ was comparable to a single Ar binding energy and was found to reproduce the experimental results more faithfully than the fully statistical model. These experimental results are plotted in Fig. 2 and compared to $D_e(CP')$ and the corresponding D_0 determined from unscaled MP2 harmonic zero point energies. Also included in Fig. 2 are dissociation energies calculated using a charge-induced dipole potential for HCO^+/Ar interactions and a Lennard-Jones potential for Ar/Ar interactions (cid/L-J) [6]. The most significant qualitative difference between the statistical and the modified statistical analysis of the experimental results occurs for the sequential binding energy of $n = 4$. Compared to $n = 3$, this binding energy is smaller with statistical analysis and larger with the modified statistical analysis. Both the $D_e(CP')$ and D_0 pattern of relative binding energies are identical to that of the modified statistical analysis providing support for that approach. Although reproducing the pattern, the MP2/pVDZ+ D_0 values are generally smaller than the modified statistical experimental results ($n = 6$ is an exception). However, the MP2/pVTZ+ results for Ar–HCO^+ and Ar_2–HCO^+ indicate that this discrepancy may be a basis set problem and that a 200–300 cm^{-1} increase in binding energy can be expected with a larger basis set. The cid/L-J binding energies are relatively independent of n and this model is not sufficient to describe fully the interactions.

Some insight into the origin of the nonmonotonic behavior of the sequential binding energies can be gained by decomposing the binding energies into a contribution from all the Ar/Ar interactions (denoted Ar shell binding) and the interaction of HCO^+ with this shell (denoted HCO^+/Ar shell binding). By construction, these two interaction energies sum to D_e. The Ar shell binding was determined by calculating

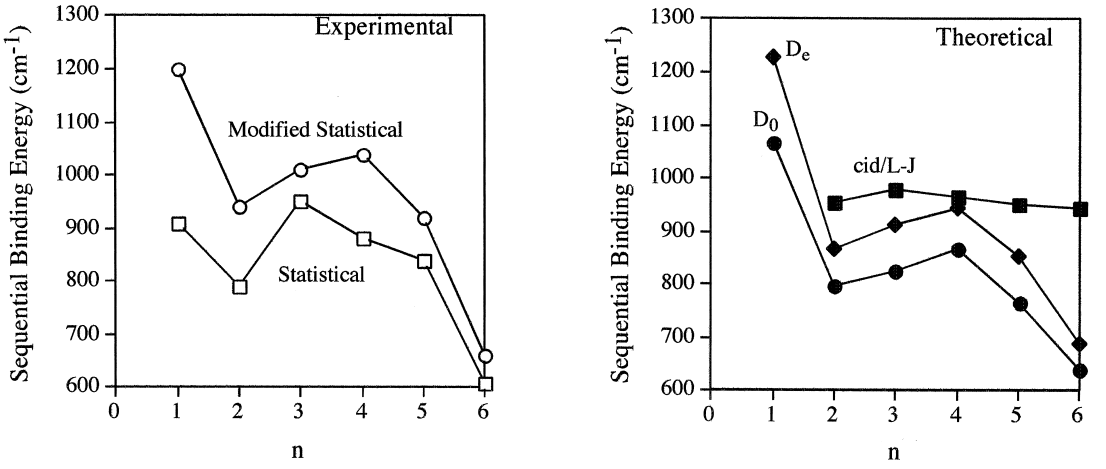

Fig. 2. Comparison of the sequential Ar binding energy for Ar_n–HCO^+ determined experimentally [6] by a statistical and a modified statistical energy randomization analysis with D_e(CP′) and the corresponding D_0 values determined from MP2/aug-cc-pVDZ calculations in the present study as a function of the number of Ar atoms (n). The cid/L-J values were determined from a model potential using a charge induced dipole potential for Ar/HCO^+ interactions and a Lennard-Jones potential for Ar/Ar interactions [6].

the interaction energy of the Ar atoms positioned in the geometry they adopt in a particular cluster ion. These energies are plotted in Fig. 3. The drop in binding energy between $n = 1$ and $n = 2$ was already appreciated in the experimental work [6] as arising from special binding position occupied the first Ar atom. The small rise in sequential binding energy occurring from $n = 2$ to $n = 4$ is due first to Ar shell binding and then split between the two types of binding. The decrease in sequential binding energy occurring from $n = 4$ to $n = 6$ is due first to a decrease in HCO^+/Ar shell binding and then to a decrease in Ar shell binding.

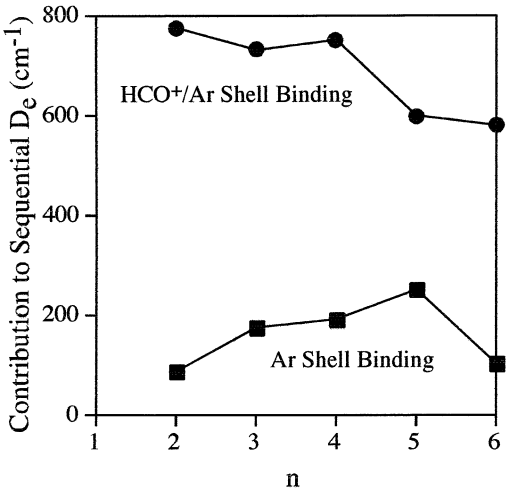

Fig. 3. Decomposition of sequential D_e(CP′) values calculated at the MP2/aug-cc-pVDZ level into a separate contribution from all Ar/Ar interactions (Ar shell binding) and Ar_n/HCO^+ interaction (HCO^+/Ar shell binding) as a function of the number of Ar atoms (n).

The pattern of Ar shell binding in Fig. 3 is relatively easy to understand in terms of the number of Ar/Ar interactions. There is one Ar/Ar interaction for $n = 2$ and the Ar shell binding is about 89 cm^{-1}. Addition of the next Ar makes two new Ar/Ar interactions and the $n = 3$ sequential Ar shell binding is about 178 cm^{-1} (i.e. twice the Ar/Ar interaction energy). The next Ar addition again makes two new Ar/Ar interactions and the $n = 4$ sequential Ar shell binding (193 cm^{-1}) is similar to the $n = 3$ value. With the fifth Ar addition, the ring is completed with three new Ar/Ar interactions and the sequential Ar shell binding is about 253 cm^{-1} (i.e. nearly three time the Ar/Ar interaction energy). The sixth Ar addition can be viewed as inserting into the Ar ring with two net new Ar/Ar interactions resulting. However, the sequential Ar shell binding is only about 107 cm^{-1}. This apparently anomalously low Ar shell binding

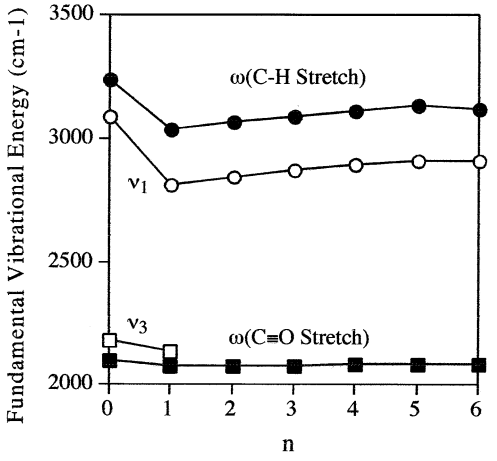

Fig. 4. Comparison of the experimental transition energy (open symbols) and MP2/aug-cc-pVDZ harmonic vibrational energies (closed symbols) for ν_1/ω(C–H stretch) and ν_3/ω(C–O stretch) as a function of the number of Ar atoms (n).

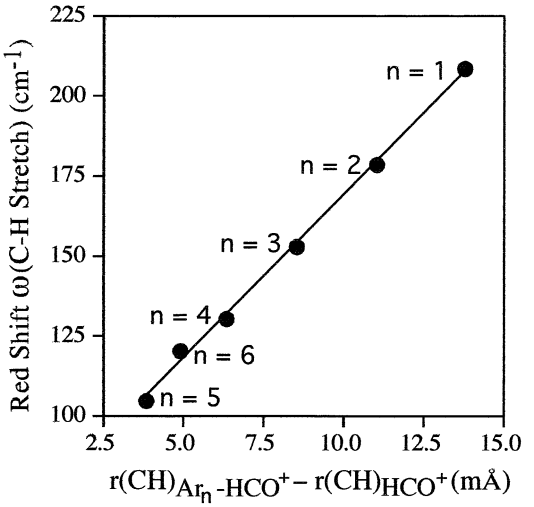

Fig. 5. Correlation of Δr_e(CH) with the redshift of ω(C–H stretch) calculated at the MP2/aug-cc-pVDZ level for Ar_n–HCO^+.

energy is caused by the repulsion generated from Ar–Ar distances in the five member ring that are more than 0.3 Å shorter than the optimal bonding distance.

The $n = 2$ to $n = 4$ sequential HCO^+/Ar shell binding energies are relatively constant averaging about 750 cm^{-1} and indicating that each of these three Ar atoms interact approximately independently with the HCO^+ ion. Somewhat surprising, the fifth and sixth sequential HCO^+/Ar shell binding energies decrease to about 590 cm^{-1} each. The reason for this drop is not completely clear but may be related to the presence of a complete symmetric Ar ring inhibiting the ability of the individual Ar atoms to take on some of the charge of the central HCO^+ ion.

4.2.3. Fundamental band energies

One of the most striking results from the experimental study [6] was the dependence of the ν_1 (C–H stretch) absorption energy on the number of Ar atoms in the cluster. As shown in Fig. 4, the first Ar addition cause a large (274 cm^{-1}) redshift in this transition which slowly blueshifted back towards the HCO^+ value with each of the next four Ar atom additions to the cluster ion. However, the sixth Ar atom addition causes a small (2.7 cm^{-1}) redshift. Qualitatively, this pattern is well reproduced by the MP2/pVDZ+ results (Fig. 4), however, the calculated harmonic frequencies are about 210–225 cm^{-1} larger than the observed transition energies for the cluster ions. Because the corresponding MP2/pVTZ+ results decrease by less than 60 cm^{-1} (Tables 2 and 3), it seems likely that the quantitative differences can be attributed to anharmonic effects.

In the experimental work, the initial large redshift followed by small incremental blueshifts as the cluster ion grew was interpreted in terms of subsequent Ar atoms pushing the first Ar atom further from the H atom and thus diminishing the Ar*–H iteration and the ensuing redshift of ν_1. Table 4 shows that this does in fact occur with the calculated results with r(Ar*–H) smoothly increasing from 2.187 Å ($n = 1$) to 2.244 Å ($n = 5$). From this point of view, the small incremental redshift observed for $n = 6$ should be accompanied by a shortening of r(Ar*–H) and Table 4 shows that this is indeed the case. However, Table 4 also indicates that the lengthening of r(Ar*–H) is associated with a shortening r(C–H); the bond length most relevant to the C–H stretching motion. The dependence of the ν_1 redshift on Δr_e(CH) is plotted in Fig. 5 where a nearly linear dependence, as expected from Badger's rule [21,22], is observed. It is particularly noteworthy that Δr_e(CH) for $n = 6$ falls between that of $n = 4$ and $n = 5$ and the redshift

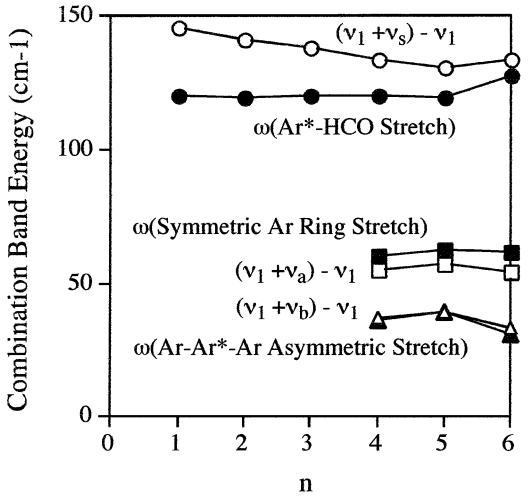

Fig. 6. Comparison of the experimental transition energy minus the ν_1 transition energy (open symbols) for three combination bands with ν_1 and MP2/aug-cc-pVDZ harmonic vibrational energies (closed symbols) for modes being assigned as those occurring in combination with ν_1 as a function of the number of Ar atoms (n).

calculated for $n = 6$ falls on nearly the same line describing the redshift dependence on Δr_e(C–H) for $n = 1$ to $n = 5$.

Experimental information is available for the ν_3 (CO stretch) band, but only with a single Ar addition [23] which is redshifted about 48 cm^{-1} with respect to ν_3 in HCO^+. This redshift is qualitatively reproduced by the MP2/pVDZ+ calculations (Fig. 4) which then indicate very little change in ω(CO) as n increases to 6. Harmonic values for the low energy vibrations of Ar–HCO^+ have been estimated from an analysis of its microwave spectra [13] and these are compared to the computational values in Table 2. The experimental estimate for the Ar*–HCO^+ stretch (ω_4 in Table 2) falls about midway between the MP2/pVDZ+ and MP2/pVTZ+ results whereas the experimental estimate for the HCO libration (ω_5 in Table 2) is about 20% below the two computational values which agree to within about 1 cm^{-1}.

4.2.4. Combination band energies

Three series of combination bands were reported for Ar_n–HCO^+ [6], all occurring in combination with ν_1. The most extensive series occurred about 130–146 cm^{-1} above ν_1 and was assigned to the Ar*–HCO^+ stretch (ν_s in the notation of [6]). Fig. 6 compares the experimental energy of $(\nu_1 + \nu_s) - \nu_1$ with the computational value of ω(Ar*–HCO^+ stretch). The general agreement lends confidence to the assignment, however, the small incremental redshift observed for $n = 1$ to $n = 5$ is not seen in the MP2/pVDZ+ results and the MP2/pVTZ+ results indicate a redshift of only about 1 cm^{-1} between $n = 1$ and $n = 2$. It might be thought that the lengthening of r(Ar*–H) with increasing number of ring Ar atoms should give rise to a redshift in this stretching frequency. However, the effect of weakening of the Ar*/H interaction with each ring Ar addition is at least partially compensated by an additional Ar*/Ar interaction. The present results cannot distinguish whether the experimental redshift with n results from anharmonic effects or computational difficulties in balancing the offsetting effects of Ar*/HCO^+ and Ar*/Ar interactions. However, the experimental blueshift occurring between $n = 5$ and $n = 6$ is qualitatively reproduced by the calculations and can be attributed to a decrease in r(Ar*–H) and an increase in r(Ar*–Ar).

The other two series of combination bands were observed only for a limited range of cluster ions. One occurred about 55–60 cm^{-1} above ν_1 for $n = 4$–7 (ν_a in the notation of [6]) and the other occurred about 30–40 cm^{-1} above ν_1 for $n = 4$–8 (ν_b in the notation of [6]). No assignment of these modes was suggested in the experimental work. To assign these modes, the eigenvectors associated with each vibration of every cluster ion was examined and labeled according to the dominate type of nuclear motion occurring. These classifications are summarized in Table 5. It was thought that candidate modes for ν_a and ν_b should (1) have vibrational energy near the experimental values, (2) correspond each to a series of similar motions, and (3) be modes that first appear for $n = 4$. Unfortunately, the calculations do not consider cluster ions large enough to apply a fourth criteria of having the modes disappear or become inactive at $n = 7$ and $n = 8$ for ν_a and ν_b, respectively. Nevertheless, reasonable assignments can be offered. Fig. 6 compares the experimental energies of $(\nu_1 + \nu_a) - \nu_1$ and $(\nu_1 + \nu_b) - \nu_1$ with the energies of ω(symmetric Ar ring stretch) and ω(Ar–

Table 5
Harmonic vibrational energy (cm^{-1}) and normal mode description for $Ar_{2,3}$, and Ar_{0-6}–HCO^+ calculated at the MP2/aug-cc-pVDZ level

Mode description	Ar_2 ($D_{\infty h}$)	Ar_3 (D_{3h})	HCO^+ ($C_{\infty v}$)	HCO^+ Ar_1 ($C_{\infty v}$)	HCO^+ Ar_2 (C_s)	HCO^+ Ar_3 (C_s)	HCO^+ Ar_4 (C_s)	HCO^+ Ar_5 (C_{4v})	HCO^+ Ar_6 (C_{5v})
Ar*									
Ar–(|)–Ar bend	···	···	···	···	···	···	17.7 (a'')	16.1 (e)	···
O								16.1 (e)	
Ar_2 stretch	25.0 (σ_g)	···	···	···	31.9 (a')	···	···	···	···
Ar_3 asymmetric stretch	···	22.4 (e')	···	···	···	22.4 (a')	26.3 (a')	20.3 (b_1)	15.5 (e_2)
		22.4 (e')				28.7 (a'')	26.5 (a'')	24.7 (b_2)	15.5 (e_2)
A–Ar*–Ar asymmetric stretch	···	···	···	···	···	···	36.7 (a'')	39.0 (e)	31.2 (e_1)
								39.0 (e)	31.2 (e_1)
Ar_3 symmetric stretch	···	31.1 (a')	···	···	···	35.8 (a')	37.7 (a')	39.6 (a_1)	38.8 (a_1)
Ar ring asymmetric stretch	···	···	···	···	···	···	···	63.1 (b_2)	43.6 (e_2)
									43.6 (e_2)
ArHCO libration	···	···	···	···	···	···	···	···	46.7 (e_1)
									46.7 (e_1)
Ar ring in-plane bend	···	···	···	···	···	···	···	···	60.9 (e_2)
									60.9 (e_2)
Ar ring symmetric stretch	···	···	···	···	···	···	60.5 (a')	62.5 (a_1)	61.8 (a_1)
H									
(C)–Ar*–Ar bend	···	···	···	···	69.8 (a')	69.2 (a'')	70.4 (a')	82.1 (e)	77.3 (e_1)
O						70.7 (a')	80.6 (a'')	82.1 (e)	77.3 (e_1)
OCH–Ar′ stretch	···	···	···	120.1 (σ)	119.8 (a')	120.5 (a')	120.7 (a')	119.4 (a_1)	127.5 (a_1)
HCO libration	···	···	···	131.0 (π)	130.2 (a'')	174.3 (a'')	178.7 (a')	213.9 (e)	182.3 (e_1)
				131.0 (π)	174.7 (a')	178.8 (a')	204.2 (a'')	213.9 (e)	182.3 (e_1)
HCO bend	···	···	835.0 (π)	920.4 (π)	887.2 (a')	882.3 (a')	861.7 (a'')	860.0 (e)	860.7 (e_1)
			835.0 (π)	920.4 (π)	915.6 (a'')	890.1 (a'')	883.8 (a')	860.0 (e)	860.7 (e_1)
CO stretch	···	···	2098.3 (σ)	2075.2 (σ)	2078.7 (a')	2081.2 (a')	2083.6 (a')	2085.8 (a_1)	2085.7 (a_1)
CH stretch	···	···	3244.2 (σ)	3035.4 (σ)	3065.0 (a')	3091.0 (a')	3113.1 (a')	3139.2 (a_1)	3123.5 (a_1)

Ar*–Ar asymmetric stretch), respectively. The very good agreement with even the small nonmonotonic variation with cluster size being essentially reproduced, satisfies criteria (1) and (2). The quality of the agreement almost certainly relies on the accident of MP2/pVDZ+ harmonic frequencies reproducing actual anharmonic transition energies for modes dominated by Ar motion. Table 5 indicates that criteria (3) is also satisfied because these modes first appear for $n = 4$, requiring at least 3/4 of a ring to be formed before these motions emerge as normal coordinates. Considering the involvement of the ring Ar atoms in this motion, it does not seem unreasonable that combinations of these modes with ν_1 would be observed for only 1–2 more Ar atom additions. The next Ar atoms would almost certainly begin to form a second ring around the "CO" end of the molecule and thereby be in a position to significantly alter the form of the normal coordinates involving the first Ar ring atoms.

5. Conclusions

Ab initio electronic structure calculations of Ar_n–HCO^+, $n = 0$–6, at the MP2/aug-cc-pVDZ level have confirmed the experimentally derived [6] conclusion that binding of an Ar atom at the hydrogen end of HCO^+ is a preferred binding site and a linear or near linear Ar–HCO^+ moiety is preserved with the binding of additional Ar atoms. The second through fifth Ar atom bind by forming a ring around the Ar–HCO^+ moiety occupying positions corresponding to the face centered lattice sites of solid argon. However, the sixth Ar atoms binds to form a five membered ring which has no analogue in the argon crystal. Sequential Ar atom binding energies are in qualitative agreement with experimental values [6] with the nonmonotonic behavior as a function of the number of Ar atoms being largely understandable when the dissociation energy is decomposed into separate contributions from Ar/Ar interactions and Ar_n/HCO^+ interactions. The experimentally observed non monotonic shift in ν_1 (C–H stretch) as a function of the number of Ar atoms [6] is qualitatively reproduced and is shown to correlate with small changes in r_e(CH) induced by Ar binding. The previous assignment [6] of a combination band with ν_1 lying about 130–146 cm^{-1} above ν_1 is confirmed and assignments are suggested for two additional experimentally observed combination bands with ν_1 which were previously unassigned.

Acknowledgements

This research was supported by the U.S. Department of Energy through the Amarillo National Resource Center for Plutonium and the Robert A. Welch Foundation.

References

[1] J.O. Hirschfelder, C.F. Curtis, R.B. Bird, Molecular Theory of Gases and Liquids, Wiley, New York, 1954.
[2] C.L. Perrin, J.B. Nielson, Annu. Rev. Phys. Chem. 48 (1997) 511.
[3] A.W. Castleman, R.G. Keesee, Chem. Rev. 86 (1986) 589.
[4] C. Lifshitz, in C.Y. Ng, T. Baer, I. Powis (Eds.), Cluster Ions, Wiley, New York, 1993.
[5] M. Meot-Ner, J. Am. Chem. Soc. 106 (1984) 1257.
[6] S.A. Nizkorodov, O. Dopfer, T. Ruchti, M. Meuwly, J.P. Maier, E.J. Bieske, J. Phys. Chem. 99 (1995) 17118.
[7] R.V. Olkhov, S.A. Nizkorodov, O. Dopfer, Chem. Phys. 239 (1998) 393.
[8] A. Nowek, J. Leszczyński, J. Chem. Phys. 105 (1996) 6388.
[9] S.F. Boys, F. Bernardi, Mol. Phys. 19 (1970) 553.
[10] A. Kumar, W.J. Meath, Can. J. Chem. 63 (1985) 1616.
[11] P.R. Herman, P.E. LaRocque, B.P. Stoicheff, J. Chem. Phys. 89 (1988) 4535.
[12] R.C. Woods, Philos. Trans. R. Soc. London, Ser. A 324 (1988) 141.
[13] Y. Ohshima, Y. Sumiyoshi, Y. Endo, J. Chem. Phys. 106 (1997) 2977.
[14] G. Chalasiński, M.M. Szcześniak, S.M. Cybulski, J. Chem. Phys. 92 (1990) 2481.
[15] R.A. Aziz, J. Chem. Phys. 99 (1993) 4518.
[16] J.M. Standard, P.R. Certain, J. Chem. Phys. 83 (1985) 3002.
[17] N.J. Wright, J.M. Hutson, J. Chem. Phys. 110 (1999) 902.
[18] G.L. Pollack, Rev. Mod. Phys. 36 (1964) 748.
[19] C.S. Gudeman, M.H. Begemann, J. Pfaff, R.J. Saykally, Phys. Rev. Lett. 50 (1983) 727.
[20] S.C. Foster, A.R.W. McKellar, T.J. Sears, J. Chem. Phys. 81 (1984) 578.
[21] R.M. Badger, J. Chem. Phys. 2 (1934) 128.
[22] R.M. Badger, J. Chem. Phys. 2 (1935) 710.
[23] H. Linnartz, T. Speck, J.P. Maier, Chem. Phys. Lett. 288 (1998) 504.
[24] K. Kawaguchi, C. Yamada, S. Saito, E. Hirota, J. Chem. Phys. 82 (1985) 1750.